Inorg. Chem. **2009**, *48*, 2246−2253

Iron(0) and Ruthenium(0) Complexes of Dinitrogen

Leslie D. Field,*,† Ruth W. Guest,†,‡ Khuong Q. Vuong,† Scott J. Dalgarno,§,|| and Paul Jensen‡

School of Chemistry, The University of New South Wales, NSW 2052, Australia, School of Chemistry, University of Sydney, NSW 2006, Australia, Department of Chemistry, University of Missouri-Columbia, Columbia, Missouri 65211, School of Engineering and Physical Sciences - Chemistry, Heriot-Watt University, Edinburgh EH14 4AS, Scotland, United Kingdom

Received October 17, 2008

The synthesis of a series of iron and ruthenium complexes with the new ligand PP^i_3 (**1**) $P(CH_2CH_2P^iPr_2)_3$ is described. The iron(0) and ruthenium(0) dinitrogen complexes $Fe(N_2)(PP^i_3)$ **(4)** and $Ru(N_2)(PP^i_3)$ **(5)** were synthesized by treatment of the iron(II) and ruthenium(II) cationic species $[FeCl(PP^i_3)]^+$ **(2)** and $[RuCl(PP^i_3)]^+$ **(3)** with potassium graphite under a nitrogen atmosphere. The cationic dinitrogen species $[Fe(N_2)H(PP^i_3)]^+$ **(6)** and $[Ru(N_2)H(PP^i_3)]^+$ **(7)** were prepared by treatment of **4** and **5**, respectively, with 1 equiv of a weak organic acid. Complexes **2**·**[BPh$_4$]**, **3**·**[BPh$_4$]**, **4**, **5**, and **6**·**[BF$_4$]** were characterized by X-ray crystallography. The structural characterization of **5** is the first report for a ruthenium(0) dinitrogen complex.

Introduction

Since the discovery of the first dinitrogen complex[1] $[Ru(NH_3)_5(N_2)]^{2+}$ in 1965, a wide variety of transition metal dinitrogen complexes have been successfully synthesized.[2−4] Many of those complexes which undergo interesting reaction chemistry contain a sterically hindered ligand environment around the metal to stabilize and protect the reactive metal center.[5−9] There is now an expanding range of sterically encumbered, polydentate ligands available, and we report here the synthesis of the hindered tripodal tetradentate phosphine ligand PP^i_3 ($P(CH_2CH_2P^iPr_2)_3$) (**1**). This ligand is a more hindered version of the PP_3 ligand skeleton, $P(CH_2CH_2PR_2)_3$, which is well-known with either phenyl[10−12] or methyl[13,14] substituents on the terminal phosphine donors.

As part of our ongoing work investigating the chemistry of coordinated dinitrogen, we have studied the synthesis and reactions of dinitrogen complexes with the PP^i_3 ligand. We report here the synthesis and characterization of the iron(0) and ruthenium(0) dinitrogen complexes $Fe(N_2)(PP^i_3)$ (**4**) and $Ru(N_2)(PP^i_3)$ (**5**), with the structural characterization of **5** being the first report of a crystal structure of a dinitrogen complex of ruthenium(0).

Results and Discussion

$P(CH_2CH_2P^iPr_2)_3$ PP^i_3 (**1**) was prepared by the base-catalyzed addition of diisopropylphosphine to trivinylphosphine in a method analogous to that used by Morris et al.[15] for the synthesis of related tripodal tetradentate phosphine ligands (Scheme 1).

* To whom correspondence should be addressed. E-mail: l.field@unsw.edu.au. Phone: +61 2 9385 2700. Fax: +61 2 9385 8008.
† The University of New South Wales.
‡ University of Sydney.
§ University of Missouri-Columbia.
|| Heriot-Watt University.

(1) Allen, A. D.; Senoff, C. V. *Chem. Commun.* **1965**, 621–622.
(2) Fryzuk, M. D.; Johnson, S. A. *Coord. Chem. Rev.* **2000**, *200−202*, 379–409.
(3) Hidai, M. *Coord. Chem. Rev.* **1999**, *185−186*, 99–108.
(4) MacKay, B. A.; Fryzuk, M. D. *Chem. Rev.* **2004**, *104*, 385–401.
(5) Laplaza, C. E.; Cummins, C. C. *Science* **1995**, *268*, 861–863.
(6) George, T. A.; Rose, D. J.; Chang, Y.; Chen, Q.; Zubieta, J. *Inorg. Chem.* **1995**, *34*, 1295–1298.
(7) Yandulov, D. V.; Schrock, R. R. *J. Am. Chem. Soc.* **2002**, *124*, 6252–6253.
(8) Betley, T. A.; Peters, J. C. *J. Am. Chem. Soc.* **2004**, *126*, 6252–6254.
(9) Fryzuk, M. D.; Johnson, S. A.; Patrick, B. O.; Albinati, A.; Mason, S. A.; Koetzle, T. F. *J. Am. Chem. Soc.* **2001**, *123*, 3960–3973.
(10) Bianchini, C.; Laschi, F.; Peruzzini, M.; Zanello, P. *Gazz. Chim. Ital.* **1994**, *124*, 271–274.
(11) King, R. B.; Kapoor, R. N.; Saran, M. S.; Kapoor, P. N. *Inorg. Chem.* **1971**, *10*, 1851–1860.
(12) Stoppioni, P.; Mani, F.; Sacconi, L. *Inorg. Chim. Acta* **1974**, *11*, 227–230.
(13) Field, L. D.; Messerle, B. A.; Smernik, R. J.; Hambley, T. W.; Turner, P. *Inorg. Chem.* **1997**, *36*, 2884–2892.
(14) Field, L. D.; Messerle, B. A.; Smernik, R. J. *Inorg. Chem.* **1997**, *36*, 5984–5990.
(15) Jia, G.; Drouin, S. D.; Jessop, P. G.; Lough, A. J.; Morris, R. H. *Organometallics* **1993**, *12*, 906–916.

10.1021/ic8019827 CCC: $40.75 © 2009 American Chemical Society
Published on Web 01/28/2009

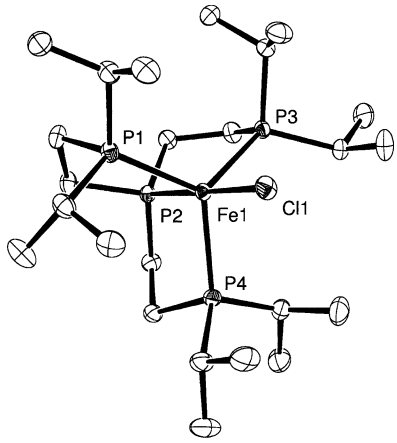

Figure 1. Oak Ridge Thermal Ellipsoid Plot (ORTEP) diagram (50% thermal ellipsoids, non-hydrogen atoms) of the complex cation of $[FeCl(PP^{i}_{3})][BPh_4]$ (**2·[BPh$_4$]**).

Scheme 1

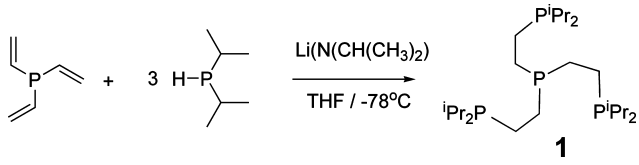

Scheme 2

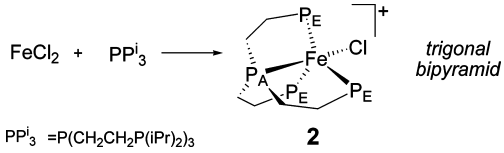

PP_3-type ligands are well established as good ligands at iron and ruthenium centers[13,14,16,17] and, in this work, the PP^{i}_{3} ligand **1** was successfully employed in the synthesis of the five coordinate chloro complexes of iron $[FeCl(PP^{i}_{3})]^{+}$ (**2**) and ruthenium $[RuCl(PP^{i}_{3})]^{+}$ (**3**).

[FeCl(PP$^{i}_{3}$)][BPh$_4$] (2·[BPh$_4$]) and [RuCl(PP$^{i}_{3}$)][BPh$_4$] (3·[BPh$_4$]). Addition of an ethanol solution of PP^{i}_{3} (**1**) to 1 equiv of iron(II) chloride resulted in the immediate formation of a dark violet solution, probably due to the paramagnetic complex [FeCl(PP$^{i}_{3}$)][Cl] **(2·Cl)**. Addition of 1 equiv of sodium tetraphenylborate precipitated the paramagnetic complex $[FeCl(PP^{i}_{3})][BPh_4]$ **(2·[BPh$_4$])** as a purple powder (Scheme 2).

Crystals of **2·[BPh$_4$]** suitable for a structure analysis were grown from a solution of THF and pentane (Figure 1). The structure of **2** approximates well to a trigonal bipyramid with the P_A-Fe-P_E angles significantly less than 90° because of the natural bite of the PP^{i}_{3} ligand. The bond lengths and bond angles (Table 1) are unexceptional and are comparable with other iron halide complexes of tetradentate phosphine ligands in the literature.[15,18]

In an analogous reaction sequence, addition of an equimolar amount of PP^{i}_{3} to a THF solution of dichlorotris(triphenylphosphine)ruthenium(II) gave a cream colored solid $[RuCl(PP^{i}_{3})][Cl]$ (**3·Cl**) which, following addition of 1 equiv of sodium tetraphenylborate in ethanol, afforded $[RuCl(PP^{i}_{3})][BPh_4]$ **(3·[BPh$_4$])** as a dark orange solid (Scheme 3). Crystals suitable for structural analysis were grown from a THF/pentane solution of **3·[BPh$_4$]** (Figure 2) and selected bond angles and bond lengths are given in Table 2.

Table 1. Selected Bond Distances and Angles for $[FeCl(PP^{i}_{3})][BPh_4]$ (**2·[BPh$_4$]**)

Bond Distances (Å)			
Fe(1)−Cl(1)	2.2371(3)	Fe(1)−P(1)	2.3694(3)
Fe(1)−P(2)	2.2182(3)	Fe(1)−P(3)	2.3558(3)
Fe(1)−P(4)	2.3940(3)		
Bond Angles (deg)			
Cl(1)−Fe(1)−P(2)	178.710(13)	Cl(1)−Fe(1)−P(1)	97.937(12)
Cl(1)−Fe(1)−P(3)	96.524(11)	Cl(1)−Fe(1)−P(4)	98.652(11)
P(2)−Fe(1)−P(1)	82.477(11)	P(2)−Fe(1)−P(3)	82.217(11)
P(2)−Fe(1)−P(4)	82.160(11)	P(1)−Fe(1)−P(3)	119.746(11)
P(1)−Fe(1)−P(4)	120.253(11)	P(3)−Fe(1)−P(4)	114.676(11)

Scheme 3

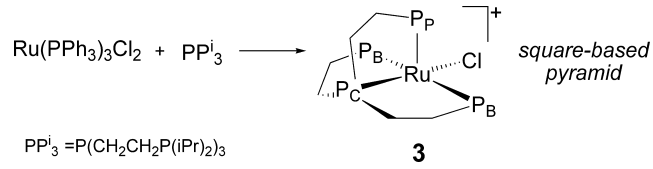

The asymmetric unit of $[RuCl(PP^{i}_{3})][BPh_4]$ **(3·[BPh$_4$])** contains two structurally similar metal centers which differ in orientation. The Ru−P_P bond length at 2.25 Å is significantly shorter than the Ru−P_B lengths at 2.38 Å, characteristic of a square-based pyramid. The Ru−P bond lengths are unremarkable in comparison with other square based pyramid ruthenium(II) complexes.[10,19] The P_B-Ru-P_B angle of **3** at 151.4° is narrower than the corresponding angles in $[RuCl_2(PPh_3)_3]$[19] (154.5°) and $[RuCl(PP^{Ph}_{3})][BPh_4]$[10] (156.4°) respectively. Thus, the polydentate ligand appears to have a restrictive effect on this angle, with the isopropyl-substituted PP^{i}_{3} of **3** more so than the phenyl-substituted PP^{Ph}_{3}.

The $^{31}P\{^{1}H\}$ NMR spectrum of **3·[BPh$_4$]** in acetone-d_6 exhibits a resonance at 144.1 ppm which is assigned to the central phosphine (P_C) and this appears as a quartet ($^{2}J_{P-P}$ = 15.4 Hz). A second broad resonance at 74.0 ppm integrates for 3 times the intensity and is assigned to the terminal phosphines at the pinnacle/base of the square-based pyramid ligand envelope. The broadening is probably due to exchange between the two inequivalent terminal phosphine environments at the base P_B and the pinnacle P_P of the pyramid structure. An analogous behavior has been described in the corresponding ruthenium complex $[RuCl(PP^{Ph}_{3})]^{+}$ (PP^{Ph}_{3} = $P(CH_2CH_2PPh_2)_3$).[10]

Fe(N$_2$)(PP$^{i}_{3}$) (4) and Ru(N$_2$)(PP$^{i}_{3}$) (5). The iron(0) and ruthenium(0) dinitrogen complexes $Fe(N_2)(PP^{i}_{3})$ (**4**) and $Ru(N_2)(PP^{i}_{3})$ (**5**) were synthesized by treatment of a THF solution of $[FeCl(PP^{i}_{3})][BPh_4]$ **(2·[BPh$_4$])** or $[RuCl(PP^{i}_{3})][Cl]$ **(3·Cl)**, respectively, with potassium graphite under an atmosphere of nitrogen (Scheme 4). After workup, **4** was obtained as a dark yellow solid, and **5** as a pale yellow solid.

(16) Bianchini, C.; Meli, A.; Peruzzini, M.; Frediani, P.; Bohanna, C.; Esteruelas, M. A.; Oro, L. A. *Organometallics* **1992**, *11*, 138–145.
(17) Bianchini, C.; Bohanna, C.; Esteruelas, M. A.; Frediani, P.; Meli, A.; Oro, L. A.; Peruzzini, M. *Organometallics* **1992**, *11*, 3837–3844.
(18) Sacconi, L.; Di Vaira, M. *Inorg. Chem.* **1978**, *17*, 810–815.
(19) La Placa, S. J.; Ibers, J. A. *Inorg. Chem.* **1965**, *4*, 778–783.

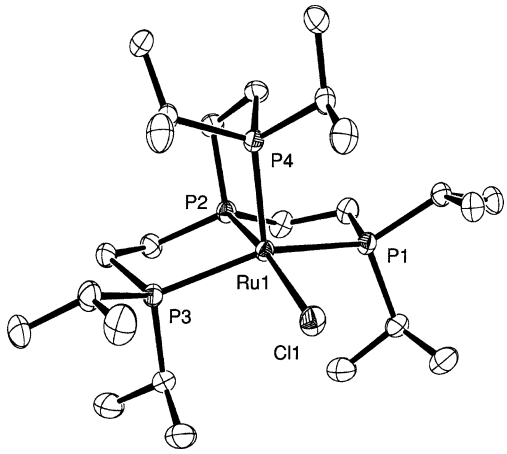

Figure 2. ORTEP diagram (50% thermal ellipsoids, non-hydrogen atoms) of one of the two complex cations of $[RuCl(PP^i_3)][BPh_4]$, **(3·BPh$_4$)**, within each asymmetric unit.

Table 2. Selected Bond Distances and Angles for $[RuCl(PP^i_3)]$ $[BPh_4]$ **(3·[BPh$_4$])**

Bond Distances (Å)			
Ru(1)−Cl(1)	2.4085(6)	Ru(1)−P(2)	2.2321(6)
Ru(1)−P(1)	2.3685(6)	Ru(1)−P(3)	2.3868(6)
Ru(1)−P(4)	2.2533(6)		
Bond Angles (deg)			
Cl(1)−Ru(1)−P(2)	167.67(2)	Cl(1)−Ru(1)−P(1)	92.98(2)
Cl(1)−Ru(1)−P(3)	94.91(2)	Cl(1)−Ru(1)−P(4)	110.03(2)
P(2)−Ru(1)−P(1)	83.97(2)	P(2)−Ru(1)−P(3)	82.49(2)
P(2)−Ru(1)−P(4)	82.28(2)	P(1)−Ru(1)−P(3)	151.38(2)
P(1)−Ru(1)−P(4)	99.20(2)	P(3)−Ru(1)−P(4)	103.80(2)

Scheme 4

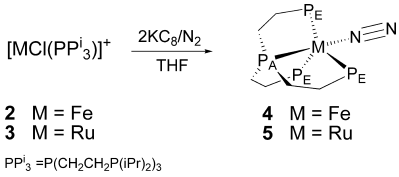

The iron(0) species **4**, unlike its iron(II) precursor **2**, is diamagnetic and has a characteristic splitting pattern in the $^{31}P\{^1H\}$ NMR spectrum for a trigonal bipyramidal complex with a tripodal tetradentate phosphine ligand such as **1**. The resonance of the apical phosphine P_A of $Fe(N_2)(PP^i_3)$ (**4**) is at relatively low field at 175.8 ppm and appears as a quartet with coupling to the 3 equivalent terminal phosphines P_E with a coupling constant of 37 Hz. The three equivalent terminal phosphines P_E appear as a doublet at 96.3 ppm with splitting due to P_A.

In the $^{31}P\{^1H\}$ NMR spectrum of the ruthenium(0) species $Ru(N_2)(PP^i_3)$ (**5**), the resonances of the apical phosphine P_A and the three equivalent terminal phosphines P_E appear as a quartet at 161.5 ppm ($^2J_{P-P}$ = 21.8 Hz) and a doublet at 88.1 ppm, respectively, with signal intensities in the ratio 1 to 3. Unlike its precursor **3**, the signals in the $^{31}P\{^1H\}$ NMR spectrum of **5** are sharp, suggestive of a trigonal bipyramidal structure in solution.

^{15}N labeling of complexes **4** and **5** was achieved by simple dinitrogen ligand exchange, following the introduction of $^{15}N_2$ gas to degassed samples of **4** and **5** in benzene-d_6. $Fe(^{15}N_2)(PP^i_3)$ (**^{15}N-4**) has a $^{31}P\{^1H\}$ NMR spectrum with chemical shifts very similar to those of **4**. The P_A resonance

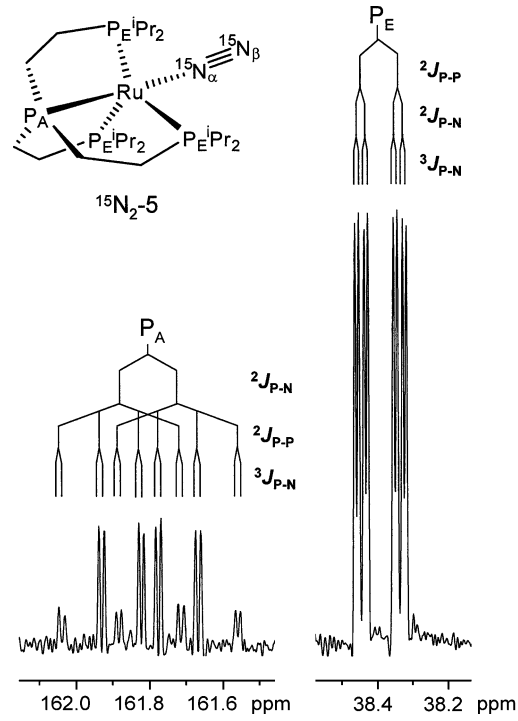

Figure 3. Resolution-enhanced $^{31}P\{^1H\}$ NMR spectrum (202 MHz, benzene-d_6) of $Ru(^{15}N_2)(PP^i_3)$ (**^{15}N$_2$-5**).

appears as a doublet of quartets with the additional doublet splitting of 10 Hz due to $^2J_{P-N}$ coupling to ^{15}N *trans* to the axial phosphine. No $^2J_{P-N}$ coupling is apparent in the P_E resonance. In the ^{15}N NMR spectrum, there are two broadened resonances at 18.1 ppm and −18.0 ppm, with equivalent intensities, which are assigned to N_β and N_α respectively on the basis of relative chemical shifts.[20]

The resolution-enhanced $^{31}P\{^1H\}$ NMR spectrum of the ^{15}N-labeled ruthenium(0) species $Ru(^{15}N_2)(PP^i_3)$ (**^{15}N-5**) (Figure 3) clearly shows additional splitting due to the coordinated $^{15}N_2$ ligand. The signal of the apical phosphorus P_A of **^{15}N$_2$-5** appears as a doublet of doublet of quartets at 161.8 ppm and that of the terminal P_E phosphorus as a doublet of doublet of doublets at 88.4 ppm. The assignment of the $^{31}P-^{15}N$ coupling constants is based on the assumption that the absolute value of the $^2J_{P-N}$ coupling is larger than the $^3J_{P-N}$ coupling.[20] The $^2J_{P-N}$ coupling constant of the P_A resonance (31.4 Hz) is significantly greater than the $^2J_{P-P}$ coupling constant (21.9 Hz) and an order of magnitude greater than the $^3J_{P-N}$ coupling constant (2.9 Hz). The order of magnitude difference between $^2J_{PN}$ and $^3J_{PN}$ *trans* coupling constants has been previously noted across the ruthenium center of a pyrazolyl phosphine complex, namely chloro-(triphenylphosphine)bis[bis(1-pyrazolyl)methane]ruthenium(II) chloride.[21] In contrast, the $^{31}P-^{15}N$ coupling constants between P_E and the coordinated dinitrogen ($^2J_{P-N}$ and $^3J_{P-N}$) are 5.2 and 2.1 Hz, respectively. It was not possible to directly measure the ^{15}N chemical shifts of **^{15}N$_2$-5**; however, the 2D $^{31}P-^{15}N$ HSQC NMR experiment

(20) Donovan-Mtunzi, S.; Richards, R. L.; Mason, J. *J. Chem. Soc., Dalton Trans.* **1984**, 469–474.
(21) Otting, G.; Messerle, B. A.; Soler, L. P. *J. Am. Chem. Soc.* **1997**, *119*, 5425–5434.

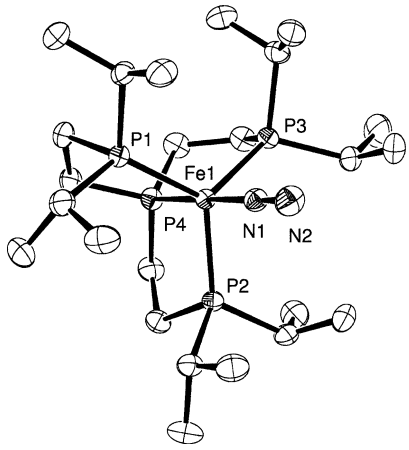

Figure 4. ORTEP diagram (50% thermal ellipsoids, non-hydrogen atoms) of $Fe(N_2)(PP^i_3)$ (**4**).

Table 3. Selected Bond Distances and Angles for $Fe(N_2)(PP^i_3)$ (**4**)

Bond Distances (Å)			
Fe(1)−N(1)	1.8032(11)	N(1)−N(2)	1.1279(16)
Fe(1)−P(4)	2.1462(4)	Fe(1)−P(1)	2.2185(4)
Fe(1)−P(2)	2.2182(4)	Fe(1)−P(3)	2.2223(4)
Bond Angles (deg)			
Fe(1)−N(1)−N(2)	179.27(12)	N(1)−Fe(1)−P(4)	179.31(4)
N(1)−Fe(1)−P(1)	95.96(4)	N(1)−Fe(1)−P(2)	94.68(4)
N(1)−Fe(1)−P(3)	94.73(4)	P(1)−Fe(1)−P(4)	84.693(15)
P(2)−Fe(1)−P(4)	84.805(16)	P(3)−Fe(1)−P(4)	85.118(15)
P(1)−Fe(1)−P(2)	121.514(15)	P(1)−Fe(1)−P(3)	118.296(15)
P(2)−Fe(1)−P(3)	117.816(14)		

provided the N_α and N_β chemical shifts as −55.3 and −8.9 ppm, respectively. No examples of ruthenium dinitrogen complexes where the resonance of N_β was designated high field with respect to N_α could be found in the literature,[20] so the higher field signal was assigned to N_α.

Yellow crystals of $Fe(N_2)(PP^i_3)$ **(4)** suitable for analysis by X-ray diffraction were precipitated from a hot pentane solution upon cooling (Figure 4). Like $[FeCl(PP^i_3)]^+$ **(2)**, this 5-coordinate species approximates well to a trigonal bipyramid. Selected bond lengths and bond angles are listed in Table 3. The average bite angle, P_A-Fe-P_E, of the tetradentate ligand is significantly less than 90° but greater than that of **2** reflecting the smaller size of the end-on bound N_2 ligand compared to chloride ligand. The N−N triple bond length of 1.13 Å indicates modest activation compared to free dinitrogen (1.10 Å).[22]

Crystals of $Ru(N_2)(PP^i_3)$ (**5**) suitable for analysis by X-ray diffraction were obtained by slow evaporation from a THF solution of **5** (Figure 5), and selected bond angles and bond lengths are given in Table 4.

The structure of **5** is a trigonal bipyramid with the three arms of the PP^i_3 ligand being equivalent by symmetry. To our knowledge this is the first structurally characterized ruthenium(0) dinitrogen complex and the first structurally characterized dinitrogen complex of ruthenium with a tripodal phosphine ligand. The N−N bond length approximates to that of free dinitrogen. This lack of activation

(22) Sutton, L. E. *Tables of Interatomic Distances and Configuration in Molecules and Ions*; The Chemical Society: London, 1958.

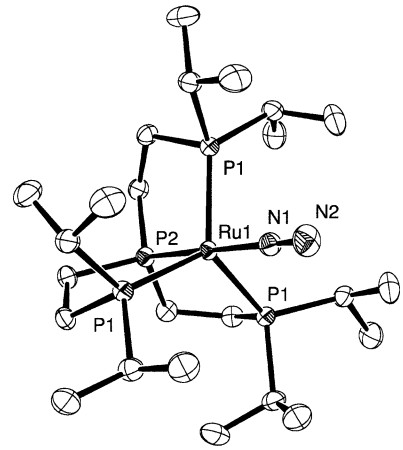

Figure 5. ORTEP diagram (50% thermal ellipsoids, non-hydrogen atoms) of $Ru(N_2)(PP^i_3)$, (**5**). The molecule has crystallographically imposed 3-fold symmetry.

Table 4. Selected Bond Distances and Angles for $Ru(N_2)(PP^i_3)$ (**5**)

Bond Distances (Å)			
Ru(1)−N(1)	1.996(3)	N(1) -N(2)	1.109(4)
Ru(1)−P(1)	2.3260(4)	Ru(1)−P(2)	2.2174(8)
Bond Angles (deg)			
Ru(1)−N(1)−N(2)	180	N(1)−Ru(1)−P(2)	180
N(1)−Ru(1)−P(1)	96.087(12)	P(1)−Ru(1)−P(2)	83.913(12)
P(1)−Ru(1)−P(1)	118.890(4)		

Scheme 5

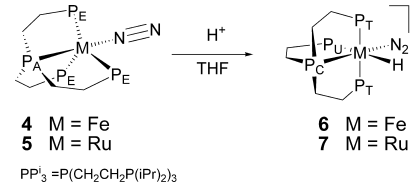

of the dinitrogen ligand suggests weak coordination which is in line with the observed facile exchange of this ligand with $^{15}N_2$.

$[Fe(N_2)H(PP^i_3)][BF_4]$ (6·$[BF_4]$) and $[Ru(N_2)H(PP^i_3)][BF_4]$ (7·$[BF_4]$). Treatment of the iron(0) and ruthenium(0) dinitrogen species **4** and **5** with 1 equiv of the weak organic acid, 2,6-lutidinium tetrafluoroborate, results in protonation of the metal centers to give the iron(II) and ruthenium(II) dinitrogen hydride complexes $[Fe(N_2)H(PP^i_3)]^+$ **(6)** and $[Ru(N_2)H(PP^i_3)]^+$ **(7)**, respectively (Scheme 5).

While the Fe(0) and Ru(0) dinitrogen complexes $Fe(N_2)(PP^i_3)$ **(4)** and $Ru(N_2)(PP^i_3)$ **(5)** both protonate with acid to form cationic hydrido complexes **(6)** and **(7)**, respectively, the ruthenium(II) complex $[Ru(N_2)H(PP^i_3)]^+$ **(7)** is stable to the acidic conditions, and no further reactions are observed. In contrast, reaction of the iron(0) complex **4** with an excess of the acid in THF results in $[Fe(N_2)H(PP^i_3)]^+$ **(6)** but also the formation of other complexes over time, and these have yet to be fully characterized.

Complex **6** is analogous to the known iron(II) dinitrogen hydride species $[Fe(N_2)H(PP_3)]^+$ (PP_3 = $P(CH_2CH_2PMe_2)_3$).[14] The $^{31}P\{^1H\}$ NMR of complexes **6** and **7** exhibit the three characteristic resonances of octahedral species of a tripodal tetradentate phosphine ligand. The central phosphine P_C signal of $[Fe(N_2)H(PP^i_3)]^+$ **(6)** at the relatively low field shift of 162.0 ppm is a doublet of triplets with a coupling

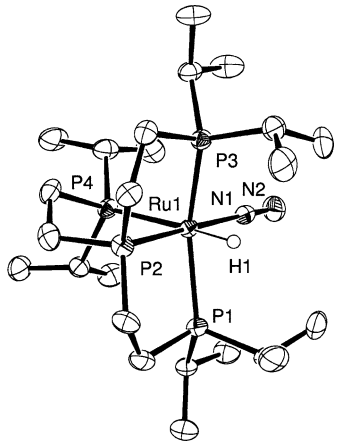

Figure 6. ORTEP diagram (50% thermal ellipsoids, selected hydrogen atoms only) of the complex cation of $[Ru(N_2)H(PP^i_3)][BF_4]\cdot THF$, **(7·[BF$_4$])**.

Table 5. Selected Bond Distances and Angles for $[Ru(N_2)H(PP^i_3)][BF_4]\cdot THF$ **(7·[BF$_4$])**

Bond Distances (Å)			
Ru(1)−N(1)	2.022(4)	N(1)−N(2)	1.092(4)
Ru(1)−P(4)	2.4236(11)	Ru(1)−P(1)	2.3538(12)
Ru(1)−P(2)	2.2522(12)	Ru(1)−P(3)	2.3523(12)
Ru(1) -H(1)	1.50(4)		
Bond Angles (deg)			
Ru(1)−N(1)−N(2)	178.7(4)	N(1)−Ru(1)−P(2)	178.91(10)
N(1)−Ru(1)−P(1)	95.30(10)	N(1)−Ru(1)−P(3)	96.44(10)
N(1)−Ru(1)−P(4)	97.95(10)	P(1)−Ru(1)−P(3)	149.67(4)
P(1)−Ru(1)−P(2)	83.98(4)	P(1)−Ru(1)−P(4)	105.24(4)
P(2)−Ru(1)−P(3)	83.82(4)	P(2)−Ru(1)−P(4)	83.03(4)
P(3)−Ru(1)−P(4)	100.70(4)		

constant to P_U and P_T of 29.8 and 24.4 Hz, respectively. The 2 equivalent terminal phosphines P_T exhibit a resonance at 88.8 ppm which appears as a doublet of doublets and has twice the intensity of the signals of P_C and P_U. The coupling constant of P_T to P_U is 11.3 Hz. The resonance of P_U appears as a well resolved doublet of triplets at 78.7 ppm. The metal-bound hydride appears as a multiplet at −14.53 ppm in the ^{1}H NMR spectrum. ^{15}N labeling of complex $[Fe(N_2)H(PP^i_3)][BF_4]$ **(6·[BF$_4$])** was achieved by dinitrogen ligand exchange, following the introduction of $^{15}N_2$ gas to a degassed sample of **6·[BF$_4$]** in THF-d_8. $[Fe(^{15}N_2)H(PP^i_3)][BF_4]$ **(^{15}N$_2$-6·[BF$_4$])** has a $^{31}P\{^1H\}$ NMR spectrum with chemical shifts almost identical to those of **6·[BF$_4$]**. The phosphine resonances appear as multiplets due to the additional $^2J_{P-N}$ and $^3J_{P-N}$ couplings. In the $^{15}N\{^1H\}$ NMR spectrum, there are two unresolved multiplets at −19.5 ppm and −51.5 ppm, with equal intensities, and these are assigned to N_β and N_α, respectively, on the basis of relative chemical shifts.

In contrast, the splitting patterns in the $^{31}P\{^1H\}$ NMR spectrum of $[Ru(N_2)H(PP^i_3)]^+$ **(7)** are not well resolved, with three resonances at 141.1, 74.7, and 62.7 ppm in the intensity ratio of 1:2:1 (P_C:P_T:P_U). The metal-bound hydride appears as a phosphorus-coupled multiplet at −11.17 ppm in the ^{1}H NMR spectrum. Yellow crystals of **7·[BF$_4$]** suitable for analysis by X-ray diffraction were obtained from a THF and pentane solution of **7·[BF$_4$]** (Figure 6), and selected bond angles and bond lengths are given in Table 5.

The bond lengths and angles of **7** are unremarkable in comparison with other ruthenium(II) structures containing tripodal phosphine ligands.[23−26] The N−N length of **7** at 1.09 Å is comparable with that of the ruthenium(0) species **5**.

Conclusions

The new sterically hindered, tripodal tetradentate ligand PP^i_3 (**1**) was synthesized and used in the synthesis of a series of stable iron and ruthenium complexes. The 5-coordinate chloro-complexes, $[FeCl(PP^i_3)]^+$ (**2**) and $[RuCl(PP^i_3)]^+$ (**3**), were reduced with potassium graphite under a dinitrogen atmosphere to give the iron(0) and ruthenium(0) dinitrogen complexes $Fe(N_2)(PP^i_3)$ (**4**) and $Ru(N_2)(PP^i_3)$ (**5**) both of which were characterized crystallographically and by multinuclear NMR spectroscopy. To our knowledge, **5** is the first report of a structurally characterized ruthenium(0) dinitrogen complex.

Treatment of the dinitrogen complexes **4** and **5** with 1 equiv of a weak organic acid led to the iron(II) and ruthenium(II) dinitrogen hydride species $[Fe(N_2)H(PP^i_3)]^+$ (**6**) and $[Ru(N_2)H(PP^i_3)]^+$ (**7**). While the ruthenium(0) dinitrogen complex **5** is relatively stable in solution and cleanly forms (**7**) in the presence of excess acid, the corresponding Fe(0) dinitrogen complex **(5)** is not and forms other species in addition to the dinitrogen hydride $[Fe(N_2)H(PP^i_3)]^+$ (**6**).

Experimental Section

General Information. All manipulations were carried out using standard Schlenk, vacuum, and glovebox techniques under a dry atmosphere of nitrogen. Solvents were dried, distilled under nitrogen or argon using standard procedures,[27] and stored in glass ampoules fitted with Youngs Teflon taps. THF and benzene were dried over sodium wire before distillation from sodium/benzophenone. Pentane was distilled from sodium/potassium alloy, while ethanol was distilled from diethoxymagnesium. THF (inhibitor free) and pentane were also dried and deoxygenated using a Pure Solv 400-4-MD (Innovative Technology) solvent purification system. Deuterated solvents THF-d_8 and benzene-d_6 were dried over, and distilled from, sodium/benzophenone and were vacuum distilled immediately prior to use. Anhydrous iron(II) chloride was purchased from Aldrich and dried before use by heating for 6 h at 120 °C under vacuum. Dichlorotris(triphenylphosphine)ruthenium(II),[28] potassium graphite,[29] and diisopropylphosphine[30] were prepared by literature methods. ^{15}N labeled dinitrogen was obtained from Cambridge Isotopes Laboratories and used without further purification. Air-sensitive NMR samples were prepared in an argon- or nitrogen-filled glovebox or on a high vacuum line by vacuum transfer of solvent into an NMR tube fitted with a concentric Teflon valve. ^{1}H spectra were recorded on Bruker Avance DRX400 or DMX600

(23) Anzellotti, A.; Briceno, A.; Delgado, G.; Diaz de Delgado, G.; Fontal, B. *Acta Crystallogr., Sect. C: Cryst. Struct. Commun.* **2002**, *58*, m355–m357.
(24) Bianchini, C.; Frediani, P.; Masi, D.; Peruzzini, M.; Zanobini, F. *Organometallics* **1994**, *13*, 4616–4632.
(25) Bianchini, C.; Masi, D.; Peruzzini, M.; Casarin, M.; Maccato, C.; Rizzi, G. A. *Inorg. Chem.* **1997**, *36*, 1061–1069.
(26) Chen, X.; Xue, P.; Sung, H. H. Y.; Williams, I. D.; Peruzzini, M.; Bianchini, C.; Jia, G. *Organometallics* **2005**, *24*, 4330–4332.
(27) Perrin, D. D. Armarego, W. L. F. *Purification of Laboratory Chemicals.*, 3rd ed.; Pergamon Press: Oxford, 1993.
(28) Hallman, P. S.; Stephenson, T. A.; Wilkinson, G. *Inorg. Synth.* **1970**, *12*, 237–240.

Table 6. Crystal Data Refinement Details for **2·[BPh$_4$]**, **3·[BPh$_4$]**, **4**, **5** and **7·[BF$_4$]**

	2·[BPh$_4$]	**3·[BPh$_4$]**	**4**	**5**	**7·[BF$_4$]**
empirical formula	$C_{48}H_{74}BClFeP_4$	$C_{48}H_{74}BClP_4Ru$	$C_{24}H_{54}FeN_2P_4$	$C_{24}H_{54}N_2P_4Ru_1$	$C_{28}H_{63}BF_4N_2OP_4Ru$
M	877.06	922.28	550.42	595.62	755.56
temp. (K)	150(2)	150(2)	173(2)	173(2)	173(2)
crystal system	monoclinic	triclinic	monoclinic	trigonal	monoclinic
space group	$P2_1/c$	$P\bar{1}$	$P2_1/n$	$R\bar{3}$	$P2_1/c$
			Unit Cell Dimensions		
a	17.6683(6)	16.107(2)	10.3494(11)	11.5137(2)	18.190(3)
b	11.3881(3)	17.156(2)	19.028(2)	11.5137(2)	12.4776(19)
c	24.6295(8)	18.102(2)	15.6727(16)	39.3998(15)	17.468(3)
α		76.756(1)			
β	105.816(2)	76.537(1)	104.437(2)		109.641(4)
γ		83.292(1)			
V (Å^3)	4768.0(3)	4724.7(10)	2988.9(5)	4523.3(2)	3734.0(10)
Z	4	4	4	6	4
ρ (calc) (g cm^{-3})	1.222	1.297	1.223	1.312	1.344
μ(Mo Kα) (mm^{-1})	0.538	0.556	0.733	0.747	0.635
N	85049	47304	21051	9574	14611
N_{ind}	18045	22021	6536	2030	7888
N_{obs} ($I > 2\sigma(I)$)	14566	17267	5832	1755	5129
*R*1(F)*	0.0329	0.0347	0.0248	0.024	0.0526
*wR*2(F^2)	0.0855	0.0919	0.0642	0.0585	0.0965

* $R1 = \sum||F_o| - |F_c||/\sum|F_o|$ for $F_o > 2\sigma(F_o)$; $wR2 = (\sum w(F_o^2 - F_c^2)^2/\sum(wF_c^2)^2)^{1/2}$ all reflections, $w = 1/[\sigma^2(F_o^2) + (0.03P)^2 + 0.2P]$ where $P = (F_o^2 + 2F_c^2)/3$.

NMR spectrometers operating at 400.13 and 600.13 MHz, respectively. ^{13}C spectra were recorded on Bruker Avance DRX400 or DMX600 NMR spectrometers operating at 100.61 or 150.92 MHz, respectively. ^{15}N NMR spectra were recorded on a Bruker DPX500 NMR spectrometer operating at 50.70 MHz. ^{31}P NMR spectra were recorded on Bruker DPX300, Avance DRX400, DPX500, or DMX600 NMR spectrometers operating at 121.49, 161.98, 202.49, and 242.95 MHz, respectively. All NMR spectra were recorded at 300 K, unless stated otherwise. ^{1}H and ^{13}C NMR spectra were referenced to solvent resonances while ^{15}N NMR spectra were referenced to external neat nitromethane at 0.00 ppm. ^{31}P NMR spectra were referenced to external neat trimethyl phosphite at 140.85 ppm. Microanalyses were carried out at the Campbell Microanalytical Laboratory, University of Otago, New Zealand. Details of the X-ray analyses are given in Table 6.

Synthesis of P(CH$_2$CH$_2$P^{i}Pr$_2$)$_3$, PP$^i_3$, (1). P(CH=CH$_2$)$_3$. Vinyl bromide (24.3 g, 0.23 mol) was condensed into THF (120 mL, −78 °C). This solution was added dropwise to a stirred suspension of magnesium turnings (3.5 g, 0.14 mol) in THF (150 mL). The reaction was initiated by addition of a crystal of iodine and warming, and after the reaction was initiated, the addition was continued at a rate that maintained the reaction at gentle reflux. After the addition was complete, the mixture was stirred at room temperature for 1 h, and trimethyl phosphite (4.15 mL, 35.2 mmol) in THF (50 mL) was added dropwise to the solution causing a gentle reflux to occur. After the addition was complete, the reaction mixture was stirred for 1 h at room temperature, and the solvent and trivinylphosphine product were distilled from the reaction mixture (68−78 °C). ^{31}P{^{1}H} NMR (243 MHz, benzene-d_6): δ −18.91 (1P, s) ppm.

PP$^i_3$ (1). Diisopropylphosphine (6 mL, 4.8 g, 41 mmol) and lithium diisopropylamide (30 mmol in 20 mL THF) were added to the cooled solution of trivinylphosphine in THF (approximately 300 mL) (−78 °C) which was then allowed to warm to room temperature with stirring. A further aliquot of diisopropylphosphine (6 mL, 4.8 g, 41 mmol) and lithium diisopropylamide (30 mmol) in THF (20 mL) was added, and the reaction mixture was stirred for a further 16 h after which time no trimethyl phosphite was present in the reaction mixture by ^{31}P{^{1}H} NMR spectroscopy. The solvent was removed under reduced pressure to afford an orange oil which was treated with methanol (30 mL). Following removal of the solvent under reduced pressure, water (20 mL) and benzene (120 mL) were added, and the resulting mixture stirred under N_2. The organic layer was separated and washed with water (2 × 10 mL) before being treated with magnesium sulfate and activated carbon. After stirring for 15 min, the benzene solution was filtered through celite. The solvent was removed under reduced pressure at 70 °C to afford **1** as a pale yellow oil (8.72 g, 53% based on trimethyl phosphite) which was used without further purification. ^{31}P{^{1}H} NMR (243 MHz, benzene-d_6): δ 9.31 (1P, d, $^3J_{P(C)\text{-}P(E)}$ = 21.7 Hz, **P$_C$**); −15.37 (3P, q, **P$_E$**) ppm. ^{1}H NMR (600 MHz, benzene-d_6): δ 1.79 (6H, m, P$_C$C**H**$_2$); 1.70, 1.62 (12H, m, P$_E$C**H**$_2$/C**H**); 1.13 (18H, dd, $^3J_{P-H}$ = 13.3 Hz, $^3J_{H-H}$ = 7.27 Hz, C**H**$_3$); 1.10 (18H, dd, $^3J_{P-H}$ = 10.9 Hz, $^3J_{H-H}$ = 7.27 Hz, C**H**$_3$) ppm. ^{13}C{^{1}H} NMR (151 MHz, benzene-d_6): δ 25.69 (apparent t, J_{P-C} = 18.3 Hz, P$_C$**C**H$_2$); 24.1 (d, $^2J_{P-C}$ = 14.7 Hz, **C**H$_3$); 19.55 (d, $^2J_{P-C}$ = 10.3 Hz, **C**H$_3$); 18.47 (dd, J_{P-C} = 13.2 Hz, J_{P-C} = 21.3 Hz, P$_E$**C**H$_2$) ppm. HRMS (EI) *m*/*z*: [M]$^+$ 467.3257 (calc. 467.3254). LRMS (ESI$^+$, methanol) *m*/*z*: 467.20 ([M+H]$^+$, 100%).

Synthesis of [FeCl(PP$^i_3$)][BPh$_4$] (2·[BPh$_4$]). Anhydrous iron(II) dichloride (0.286 g, 2.26 mmol) was added to PP$^i_3$ **1** (1.05 g, 2.24 mmol) in ethanol (approximately 25 mL) under nitrogen. The reaction mixture, which immediately developed a dark violet color, was left to stir under nitrogen for 18 h. Sodium tetraphenylborate (0.900 g, 2.60 mmol) was added, resulting in the immediate precipitation of a violet solid which was isolated by filtration to give the paramagnetic title compound [FeCl(PP$^i_3$)][BPh$_4$] **2·[BPh$_4$]** as a purple powder (1.83 g, 93%). Crystals suitable for X-ray diffraction were grown by layering a THF solution of the complex with pentane. Anal. Found: C 65.72, H 8.29 $C_{48}H_{74}BClFeP_4$ (MW 877.11) requires C 65.73, H 8.50%. HRMS (EI) *m*/*z*: [M]$^+$ 557.2210 (calc. 557.2214). LRMS (ESI$^+$, methanol) *m*/*z*: 557 ([M+H]$^+$, 100%), 467 ([PP$^i_3$+H]$^+$, 35).

Synthesis of [RuCl(PP$^i_3$)][BPh$_4$] (3·[BPh$_4$]). Dichlorotris(triphenylphosphine)ruthenium(II) (0.78 g, 0.82 mmol) and PP$^i_3$ **1** (0.38 g, 0.82 mmol) were stirred in THF (approximately 25 mL). A red solution formed immediately followed by the precipitation of a

(29) Weitz, I. S.; Rabinovitz, M. *J. Chem. Soc., Perkin Trans. 1* **1993**, 117–120.
(30) Zhu, K.; Achord, P. D.; Zhang, X.; Krogh-Jespersen, K.; Goldman, A. S. *J. Am. Chem. Soc.* **2004**, *126*, 13044–13053.

cream colored solid after approximately 5 min. The solid was isolated by filtration and washed with THF to give [RuCl(PP^i_3)]Cl (392 mg, 80%). $^{31}P\{^1H\}$ NMR (162 MHz, ethanol): δ 142.9 (1P, q, $^2J_{P(C)\text{-}P(B/P)}$ = 15.2 Hz, $\mathbf{P_C}$); 72.1 (3P, d, $\mathbf{P_{B/P}}$) ppm. HRMS (EI) *m/z*: $[M]^+$ 603.1909 (calc. 603.1908). LRMS (ESI^+, methanol) *m/z*: 621 ($[RuCl(PP^i_3)+H_2O]^+$, 100%), 619 ($[RuCl(PP^i_3)+OH]^+$, 95), 603 ($[RuCl(PP^i_3)+H]^+$, 56), 517 (68).

Sodium tetraphenylborate (60 mg, 180 μmol) was added to a solution of [RuCl(PP^i_3)]Cl (104 mg, 163 μmol) in ethanol (approximately 10 mL) resulting in the immediate formation of a dark orange precipitate. The precipitate was isolated by filtration and washed with ethanol to give [RuCl(PP^i_3)][BPh_4] **3·[BPh$_4$]** (135 mg, 90%) as a dark orange powder. Crystals suitable for X-ray diffraction were grown by layering a THF solution of **3·[BPh$_4$]** with pentane. Anal. Found: C 62.29, H 7.97 $C_{48}H_{74}BClP_4Ru$ (MW 922.33) requires C 62.51, H 8.09%. $^{31}P\{^1H\}$ NMR (162 MHz, acetone-d_6): δ 144.1 (1P, q, $^2J_{P(A)\text{-}P(B/P)}$ = 15.4 Hz, $\mathbf{P_A}$); 74.0 (3P, br s, $\mathbf{P_{B/P}}$) ppm. $^1H\{^{31}P\}$ NMR (400 MHz, acetone-d_6): δ 7.38 (8H, br m, B$\mathbf{Ph_{ortho}}$); 6.97 (8H, m, B$\mathbf{Ph_{meta}}$); 6.82 (4H, m, B$\mathbf{Ph_{para}}$); 2.32 (6H, t, $^3J_{H-H}$= 7.2 Hz, $P_C\mathbf{CH}_2$); 2.17 (6H, h, $^3J_{H-H}$= 7.3 Hz, $P_{B/P}\mathbf{CH}(CH_3)_2$); 2.17 (6H, m, $P_{B/P}\mathbf{CH}_2$); 1.55 (18H, d, $\mathbf{CH}_3$); 1.20 (18H, d, $\mathbf{CH}_3$) ppm. $^{13}C\{^1H\}$ NMR (101 MHz, acetone-d_6): δ 164.9 (m, B$\mathbf{Ph_{ipso}}$); 136.8 (s, B$\mathbf{Ph_{ortho}}$); 125.7 (m, B$\mathbf{Ph_{meta}}$); 122.0 (s, B$\mathbf{Ph_{para}}$); 30.0 (m, $P_E\mathbf{C}H(CH_3)_2$); 26.2 (m, $P_E\mathbf{C}H_2$); 25.9 (d, $^1J_{C-P}$= 30.5 Hz, $P_A\mathbf{C}H_2$); 19.7 (s, $\mathbf{C}H_3$); 19.5 (s, $\mathbf{C}H_3$) ppm.

Synthesis of Fe(N_2)(PP^i_3) (4). Potassium graphite (75 mg, 0.55 mmol) was added to a solution of **2·[BPh$_4$]** (230 mg, 0.262 mmol) in THF (approximately 15 mL). The reaction mixture was stirred under nitrogen for 24 h. The resulting black suspension was filtered to give an orange solution. The solvent was removed under reduced pressure, and the solid residue extracted into pentane (approximately 10 mL). The yellow solution was filtered, and the solvent removed under reduced pressure to give Fe(N_2)(PP^i_3) **4** as a dark yellow solid (75 mg, 52%). Crystals suitable for analysis by X-ray diffraction were precipitated upon cooling of a hot pentane solution of **4**. Anal. Found: C 52.31, H 9.93, N 3.85, $C_{24}H_{54}FeN_2P_4$ (MW 550.44) requires C 52.37, H 9.89, N 5.09%. Elemental analysis performed on crystalline product suggests some loss of weakly bound dinitrogen ligand upon application of vacuum during analytical procedure. $^{31}P\{^1H\}$ NMR (162 MHz, benzene-d_6): δ 175.8 (1P, q, $^2J_{P(A)\text{-}P(E)}$ = 36.7 Hz, $\mathbf{P_A}$); 96.3 (3P, d, $\mathbf{P_E}$) ppm. $^1H\{^{31}P\}$ NMR (400 MHz, benzene-d_6): δ 2.29 (6H, m, $P_E\mathbf{C}H(CH_3)_2$); 1.35 (6H, m, $P_A\mathbf{C}H_2$); 1.28 (18H, m, $\mathbf{C}H_3$); 1.25 (18H, m, $\mathbf{C}H_3$); 1.10 (6H, m, $P_E\mathbf{C}H_2$) ppm. $^{13}C\{^1H\}$ NMR (101 MHz, benzene-d_6): δ 34.3 (m, $\mathbf{C}H_3$); 29.0 (m, $P_E\mathbf{C}H_2$); 28.8 (m, $P_A\mathbf{C}H_2$); 20.5 (d, $^1J_{C-P}$ = 11 Hz, $P_E\mathbf{C}H(CH_3)_2$) ppm. IR (fluorolube): ν 1985 s (N≡N) cm^{-1}. LRMS (ESI^+, methanol) *m/z*: 523 ($[Fe(PP^i_3)+H]^+$, 100%), 522 (81).

Fe($^{15}N_2$)(PP^i_3) ($^{15}N_2$-4) (NMR Scale). Fe(N_2)(PP^i_3) **4** (approximately 20 mg, 80 μmol) was dissolved in benzene-d_6 (0.5 mL) in an NMR tube fitted with a concentric Teflon valve under dinitrogen. The solution was frozen in liquid nitrogen, and the headspace was evacuated followed by introduction of $^{15}N_2$ to the NMR tube. NMR spectra indicated the successful exchange of the dinitrogen ligand following thawing of the solution and warming to room temperature. $^{31}P\{^1H\}$ NMR (202 MHz, benzene-d_6): δ 175.6 (1P, dq $^2J_{P(A)\text{-}(E)}$ = 36.7 Hz, $^2J_{P(A)\text{-}N}$ = 9.7 Hz, $\mathbf{P_A}$,); 96.1 (3P, d, $\mathbf{P_E}$) ppm. ^{15}N NMR (50.7 MHz, benzene-d_6) δ 18.1 (1N, Fe−N**N**); −18.0 (1N, Fe-**N**) ppm.

Synthesis of Ru(N_2)(PP^i_3) (5). Potassium graphite (109 mg, 0.81 mmol) was added to a suspension of [RuCl(PP^i_3)]Cl **3·Cl** (144 mg, 0.226 mmol) in THF (approximately 15 mL). The reaction mixture was stirred under nitrogen for 18 h after which it was filtered to give a dark yellow solution. The solvent was removed under reduced pressure, and the resulting dark yellow solid was dissolved in pentane, filtered, and the solvent removed under reduced pressure to give Ru(N_2)(PP^i_3) **5** (90 mg, 67%) as a yellow solid. Anal. Found: C 48.66, H 9.37, N 4.38 $C_{24}H_{54}N_2P_4Ru$ (MW 595.64) requires C 48.39, H 9.14, N 4.70%. $^{31}P\{^1H\}$ NMR (162 MHz, benzene-d_6): δ 161.5 (1P, q, $^2J_{P(A)\text{-}P(E)}$ = 21.8 Hz, $\mathbf{P_A}$); 88.1 (3P, d, $\mathbf{P_E}$) ppm. $^1H\{^{31}P\}$ NMR (400 MHz, benzene-d_6): δ 2.11 (6H, m, $^3J_{H-H}$ = 7.2 Hz, $P_E\mathbf{C}H(CH_3)_2$); 1.27 (6H, m, $P_A\mathbf{C}H_2$); 1.28 (18H, d, $\mathbf{C}H_3$); 1.16 (6H, m, $P_E\mathbf{C}H_2$); 1.13 (18H, m, $\mathbf{C}H_3$) ppm. $^{13}C\{^1H\}$ NMR (101 MHz, benzene-d_6): δ 33.8 (m, $P_E\mathbf{C}H(CH_3)_2$); 30.1−29.3 (m, $P_A\mathbf{C}H_2\mathbf{C}H_2$); 20.4 (s, $P_E\mathbf{C}H(CH_3)_2$); 20.2 (s, $P_E\mathbf{C}H(CH_3)_2$) ppm. IR (fluorolube): 2083 s, ν(N≡N) cm^{-1}.

Ru($^{15}N_2$)(PP^i_3) ($^{15}N_2$-5) (NMR Scale). Ru(N_2)(PP^i_3) **5** (approx 20 mg, 80 μmol) was dissolved in benzene-d_6 (0.5 mL) in an NMR tube fitted with a concentric Teflon tap under dinitrogen. The solution was frozen with liquid nitrogen, and the headspace evacuated followed by introduction of $^{15}N_2$ to the NMR tube. NMR spectra indicated the successful exchange of the dinitrogen ligand following thawing of the solution and warming to room temperature. $^{31}P\{^1H\}$ NMR (202 MHz, benzene-d_6): δ 161.8 (1P, ddq, $\mathbf{P_A}$, $^2J_{P(A)\text{-}N}$ = 31.4 Hz, $^2J_{P(A)\text{-}P(E)}$ = 21.9 Hz, $^3J_{P(A)\text{-}N}$ = 2.9 Hz); 88.4 (3P, ddd, $\mathbf{P_E}$, $^2J_{P(E)\text{-}N}$ = 5.2 Hz, $^3J_{P(E)\text{-}N}$ = 2.1 Hz) ppm. ^{15}N NMR (50.7 MHz, benzene-d_6) δ −8.9 (1N, Ru−N**N**); −55.3 (1N, Ru-**N**N) ppm (by $^{31}P-^{15}N$ HSQC).

Synthesis of [Fe(N_2)H(PP^i_3)][BF_4] (6·BF_4). Fe(N_2)(PP^i_3) **4** (20 mg, 36 μmol) and 2,6-lutidinium tetrafluoroborate (7 mg, 36 μmol) were stirred in THF (approximately 2 mL) under nitrogen to afford a red solution which turned purple within an hour. The solution was layered with pentane, and after 24 h the resulting solid was isolated by filtration to give [Fe(N_2)H(PP^i_3)][BF_4] **6·[BF$_4$]** as a purple solid (16 mg, 70%). $^{31}P\{^1H\}$ NMR (121.5 MHz, THF-d_8): δ 162.0 (1P, dt, $^2J_{P(C)\text{-}P(U)}$ = 29.8 Hz, $^2J_{P(C)\text{-}P(T)}$ = 24.4 Hz, $\mathbf{P_C}$); 88.8 (2P, dd, $^2J_{P(T)\text{-}P(U)}$ = 11.3 Hz, $\mathbf{P_T}$); 78.7 (1P, dt, $\mathbf{P_U}$) ppm. $^1H\{^{31}P\}$ NMR (400 MHz, THF-d_8): δ 2.6−2.4 (8H, m, $P_T\mathbf{C}H_2\mathbf{C}H_2$); 2.57 (2H, m, $P_T\mathbf{C}H$); 2.15 (2H, m, $P_U\mathbf{C}H$); 2.10−1.80 (4H, m, $P_U\mathbf{C}H_2\mathbf{C}H_2$); 1.73 (2H, m, $P_T\mathbf{C}H'$);1.50 (6H, d, $^3J_{H-H}$ = 7 Hz, $P_UCH(\mathbf{C}H_3)$); 1.41 (6H, d, $^3J_{H-H}$ = 7 Hz, $P_TCH(\mathbf{C}H_3)$); 1.34 (6H, d, $^3J_{H-H}$ = 7 Hz, $P_UCH(\mathbf{C}H_3)$); 1.31 (6H, d, $^3J_{H-H}$ = 7 Hz, $P_TCH(\mathbf{C}H_3)$); 1.27 (6H, d, $^3J_{H-H}$ = 7 Hz, $P_TCH'(\mathbf{C}H_3)$); 1.13 (6H, d, $^3J_{H-H}$ = 7 Hz, $P_TCH'(\mathbf{C}H_3)$); −14.53 (1H, s, Fe-**H**) ppm. ^1H NMR (400 MHz, THF-d_8, high field): δ −14.53 (1H, ddt, Fe-**H,** $^2J_{H-P(T)}$ = 67.2 Hz, $^2J_{H-P(C)}$ = 51.7 Hz, $^2J_{H-P(U)}$ = 24.4 Hz) ppm. IR (fluorolube): 2095 s, ν(N≡N) cm^{-1}.

[Fe($^{15}N_2$)H(PP^i_3)][BF_4] ([$^{15}N_2$-6][BF_4]) (NMR Scale). An NMR sample of **6·**[BF_4] was prepared by addition of 2,6-lutidinium tetrafluoroborate (16 mg, 82 μmol) to a solution of Fe(N_2)(PP^i_3) **(4)** (44 mg, 80 μmol) in THF-d_8 (0.5 mL) in an NMR tube fitted with a concentric Teflon tap under dinitrogen. The resulting solution of **6·[BF$_4$]** was frozen in liquid nitrogen, and the headspace was evacuated followed by introduction of $^{15}N_2$ to the NMR tube. NMR spectra indicated the successful exchange of the dinitrogen ligand following thawing of the solution and warming to room temperature. $^{31}P\{^1H\}$ NMR (162 MHz, THF-d_a): δ 161.9 (1P, m, $^2J_{P(C)\text{-}P(U)}$ = 30 Hz, $^2J_{P(C)\text{-}P(T)}$ = 24 Hz, $\mathbf{P_C}$); 88.6 (2P, m, $^2J_{P(T)\text{-}P(U)}$ = 11 Hz, $\mathbf{P_T}$); 78.5 (1P, m, $\mathbf{P_U}$) ppm. $^{15}N\{^1H\}$ NMR (40.6 MHz, THF-d_a) δ −19.5 (1N, Fe−N**N**); −51.5 (1N, Fe-**N**) ppm. ^1H NMR (400 MHz, THF-d_8, high field): δ −14.5 (1H, ddt, Fe-**H,** $^2J_{H-P(T)}$ = 67 Hz, $^2J_{H-P(C)}$ = 52 Hz, $^2J_{H-P(U)}$ = 24 Hz) ppm.

Synthesis of [Ru(N_2)H(PP^i_3)][BF_4] (7·[BF_4]). 2,6-Lutidinium tetrafluoroborate (17 mg, 100 μmol) was added to a solution of Ru(N_2)(PP^i_3) **5** (60 mg, 100 μmol) in THF (approximately 15 mL). The solution turned green for several minutes before reverting to

yellow. After stirring for an hour, the solution was filtered, and the volume reduced under reduced pressure to approximately 2 mL. This solution was layered with pentane to afford yellow crystals of $[Ru(N_2)H(PP^i{}_3)][BF_4]$ **7·[BF$_4$]** (52 mg, 75%). Anal. Found: C 42.41, H 7.82, N 3.85, $C_{24}H_{55}BF_4N_2P_4Ru$ (MW 683.48) requires C 42.18, H 8.11, N 4.10%. $^{31}P\{^1H\}$ NMR (122 MHz, 298 K, THF-d_8): δ 143.1 (1P, m, $\mathbf{P_C}$); 74.7 (2P, m, $\mathbf{P_T}$); 62.7 (2P, m, $\mathbf{P_U}$) ppm. $^1H\{^{31}P\}$ NMR (400 MHz, THF-d_8): δ 2.6−2.4 (6H, m, $P_CC\mathbf{H}_2$); 2.07 (2H, m, $P_TC\mathbf{H}$); 2.49 (2H, m, $P_TC\mathbf{H}'$); 2.07 (2H, m, $P_UC\mathbf{H}$); 1.80 (2H, m, $P_UC\mathbf{H}_2$); 1.71 (4H, m, $P_TC\mathbf{H}_2$); 1.44 (6H, d, $^3J_{H-H}$ = 7.6 Hz, $P_UCH(C\mathbf{H}_3)$); 1.33 (6H, d, $^3J_{H-H}$ = 7.4 Hz, $P_UCH(C\mathbf{H}_3)$); 1.38 (6H, d, $^3J_{H-H}$ = 7.0 Hz, $P_TCH(C\mathbf{H}_3)$), 1.29 (6H, d, $^3J_{H-H}$ = 6.6 Hz, $P_TCH(C\mathbf{H}_3)$); 1.23 (6H, d, $^3J_{H-H}$ = 6.5 Hz, $P_TCH'(C\mathbf{H}_3)$); 1.08 (6H, d, $^3J_{H-H}$ = 6.7 Hz, $P_TCH'(C\mathbf{H}_3)$); −11.17 (1H, s, Ru-**H**) ppm. IR (fluorolube): 2171 s, ν(N≡N) cm^{-1}.

Acknowledgment. The authors thank the Australian Research Council for financial support and Dr Hsiu Lin Li (University of New South Wales) for valuable assistance with manipulation and characterization of air sensitive compounds.

Supporting Information Available: A CIF file giving crystallographic data. This material is available free of charge via the Internet at http://pubs.acs.org.

IC8019827